The Astrophysical Journal, 776:20 (12pp), 2013 October 10 doi:10.1088/0004-637X/776/1/20

PSR J1723−2837: AN ECLIPSING BINARY RADIO MILLISECOND PULSAR

Fronefield Crawford[1], Andrew G. Lyne[2], Ingrid H. Stairs[3], David L. Kaplan[4,5], Maura A. McLaughlin[6], Paulo C. C. Freire[7], Marta Burgay[8], Fernando Camilo[9,10], Nichi D'Amico[8], Andrew Faulkner[11], Michael Kramer[7], Duncan R. Lorimer[6,14], Richard N. Manchester[12], Andrea Possenti[8], and Danny Steeghs[13]
[1] Department of Physics and Astronomy, Franklin and Marshall College, P.O. Box 3003, Lancaster, PA 17604, USA; fcrawfor@fandm.edu
[2] Jodrell Bank Centre for Astrophysics, University of Manchester, Manchester M13 9PL, UK
[3] Department of Physics and Astronomy, University of British Columbia, 6224 Agricultural Road, Vancouver, BC V6T 1Z1, Canada
[4] Physics Department, University of Wisconsin - Milwaukee, Milwaukee, WI 53211, USA
[5] Department of Astronomy, University of Wisconsin - Madison, Madison, WI 53715, USA
[6] Department of Physics, West Virginia University, Morgantown, WV 26506, USA
[7] Max-Planck-Institut für Radioastronomie, auf dem Huegel 69, D-53121 Bonn, Germany
[8] INAF - Osservatorio Astronomico di Cagliari, Poggio dei Pini, I-09012 Capoterra, Italy
[9] Columbia Astrophysics Laboratory, Columbia University, New York, NY 10027, USA
[10] Arecibo Observatory, HC3 Box 53995, Arecibo, PR 00612, USA
[11] Cavendish Laboratory, University of Cambridge, J. J. Thompson Avenue, Cambridge, CB3 0HE, UK
[12] CSIRO Astronomy and Space Science, Australia Telescope National Facility, P.O. Box 76, Epping, NSW 1710, Australia
[13] Department of Physics, University of Warwick, Coventry CV4 7AL, UK
Received 2013 May 6; accepted 2013 August 21; published 2013 September 20

ABSTRACT

We present a study of PSR J1723−2837, an eclipsing, 1.86 ms millisecond binary radio pulsar discovered in the Parkes Multibeam survey. Radio timing indicates that the pulsar has a circular orbit with a 15 hr orbital period, a low-mass companion, and a measurable orbital period derivative. The eclipse fraction of ∼15% during the pulsar's orbit is twice the Roche lobe size inferred for the companion. The timing behavior is significantly affected by unmodeled systematics of astrophysical origin, and higher-order orbital period derivatives are needed in the timing solution to account for these variations. We have identified the pulsar's (non-degenerate) companion using archival ultraviolet, optical, and infrared survey data and new optical photometry. Doppler shifts from optical spectroscopy confirm the star's association with the pulsar and indicate a pulsar-to-companion mass ratio of 3.3 ± 0.5, corresponding to a companion mass range of 0.4 to 0.7 $M_\odot$ and an orbital inclination angle range of between 30° and 41°, assuming a pulsar mass range of 1.4–2.0 $M_\odot$. Spectroscopy indicates a spectral type of G for the companion and an inferred Roche-lobe-filling distance that is consistent with the distance estimated from radio dispersion. The features of PSR J1723−2837 indicate that it is likely a "redback" system. Unlike the five other Galactic redbacks discovered to date, PSR J1723−2837 has not been detected as a γ-ray source with *Fermi*. This may be due to an intrinsic spin-down luminosity that is much smaller than the measured value if the unmeasured contribution from proper motion is large.

Key words: binaries: eclipsing – pulsars: individual (PSR J1723−2837)

Online-only material: color figures

1. INTRODUCTION

In the standard model for millisecond pulsar (MSP) production (Alpar et al. 1982), old neutron stars are recycled by the accretion of matter from a companion star. This model predicts that the longer this phase of the evolution lasts, the shorter the period of the resulting MSP will be. During the accretion phase, copious X-ray emission is produced, and the neutron star is observed as a low-mass X-ray binary (LMXB) in cases where the mass of the companion is small. After the accretion phase is finished and the pulsar has been spun up, the neutron star may emit detectable radio pulses and be observable as an MSP with an evolved white dwarf companion. This evolutionary path from LMXB to radio MSP is important to verify and understand. The discovery of the first accretion-powered MSP in X-rays, SAX 1808.4−3658 (Wijnands & van der Klis 1998; Chakrabarty & Morgan 1998), suggested this connection. However, objects that are actually undergoing a transition between an LMXB phase and a radio MSP phase further solidify this link, but these systems are rare. It was not until the discovery of PSR J1023+0038 by Archibald et al. (2009) that a transition object was discovered. Since then, a total of five objects (called "redbacks") having similar companion characteristics and eclipsing behavior have been discovered in our Galaxy (Roberts 2013). In 2013, a redback system in the globular cluster (GC) M28, PSR J1824−2452I, was found to swing between being a radio MSP and an LMXB with detectable X-ray pulsations at the exact period and orbital characteristics of the radio pulsar (an accretion-powered MSP). It then went back to being a radio MSP, confirming the evolutionary link beyond doubt and establishing the existence of an intermediate phase where the accretion and radio MSP phases alternate on very short timescales (Papitto et al. 2013).

PSR J1723−2837 is a radio MSP that was discovered by Faulkner et al. (2004) in the Parkes multibeam pulsar survey. It has a spin period of 1.86 ms, making it the 12th most rapidly rotating radio pulsar currently listed in the ATNF Pulsar Catalogue (Manchester et al. 2005).[15] From the original survey detection, it was clear that the pulsar was highly accelerated and flux-variable, making it difficult to detect despite being very bright at certain orbital phases. In this paper we present and

[14] Adjunct Astronomer at the National Radio Astronomy Observatory

[15] http://www.atnf.csiro.au/research/pulsar/psrcat/, V1.46

Table 1
Timing Observations of PSR J1723−2837

Telescope	Backend	Center Freq. (MHz)	N_{TOA}[a]	MJD Range	TEMPO[b] EFAC	Detection[c] Percentage
GBT	GUPPI	2000	234	55102–55263	2.15	75%
Jodrell Bank	DFB	1520	138	55196–55803	14	30%
Parkes	PDFB4	1369	2	55292	1	50%
	PDFB4	3100	10	55297–55312	1	80%

Notes.
[a] Number of TOAs used in the timing fit. Multiple TOAs were generated from each GBT and Parkes observation.
[b] TOA uncertainties from each instrumental setup were multiplied by this factor to correct for the generally underestimated uncertainties produced by the program that generates the TOAs.
[c] Approximate percentage of timing observations in which the pulsar was detected.

discuss the timing results for PSR J1723−2837 and optical observations that identify and characterize the pulsar's companion. PSR J1723−2837 is the sixth Galactic redback yet discovered, and this number will most likely grow as radio surveys continue to detect new pulsar systems identified in *Fermi* γ-ray observations (Ray et al. 2012).

The paper is laid out as follows. In Section 2, we describe the timing observations of PSR J1723−2837, and in Section 3 we present the timing results. In Section 4, we describe archival and new optical and infrared observations that identify the companion star and demonstrate its association with the pulsar. Section 5 presents a discussion of the system, and Section 6 presents our conclusions and summarizes our results.

2. TIMING OBSERVATIONS

Between 2001 March, when PSR J1723−2837 was discovered, and 2004 September, the pulsar was only sporadically detected in 1400 MHz observations that were attempted with the Parkes 64 m telescope. In 2009 September, we made several new detections with exploratory observations at 2000 MHz using the Robert C. Byrd Green Bank Telescope (GBT). We derived a preliminary orbital ephemeris from these Parkes and GBT detections using a method described by Freire et al. (2001) which uses the measured spin periods and accelerations of the pulsar and is well-suited for cases where detections are sparse. Using this new orbital solution, timing observations resumed in 2009 December with the Jodrell Bank 76 m Lovell telescope and in 2010 February with the GBT. Between 2009 September and 2011 March, the pulsar was detected regularly at frequencies of 1520 MHz (with Jodrell), 2000 MHz (with the GBT), and also several times at 1369 and 3100 MHz (with Parkes). These observations were used to obtain a phase-connected timing solution, which we present here. For all of the observations discussed, dual polarizations were summed at the telescope prior to data recording and analysis.

Observations with the GBT used the Green Bank Ultimate Processing Instrument (GUPPI) to observe the pulsar at 2000 MHz in a number of sessions. In these observations, a bandwidth of 800 MHz was split into 2048 filterbank channels, each of which was sampled at 64 μs. Integration times ranged from about 30 minutes to 2 hr. Multiple times-of-arrival (TOAs) were derived from each observation using the PRESTO software package (Ransom 2001; Ransom et al. 2002). Sub-integrations from each observation were dedispersed and folded, and the resulting profiles were compared to a pulse profile template produced from one of the strong detections. PSR J1723−2837 was also observed regularly at a center frequency of 1520 MHz with the Lovell telescope. These observations used a cryogenically cooled receiver and a digital filterbank backend with 384 MHz of bandwidth split into 1536 frequency channels of width 0.25 MHz. The sampling time was 128 samples per pulse period, or 14.5 μs. Typical integration times were between 30 and 40 minutes per observation. TOAs were produced from these observations, and the first phase-connected timing solution was made with these data. In 2010 April, Parkes observations were conducted for seven sessions with the PDFB4 digital backend. Two of these sessions were conducted at a center frequency of 1369 MHz, and five were at 3100 MHz. One 1369 MHz detection and four 3100 MHz detections were made from these observations, and TOAs were produced and included in the timing solution. Table 1 shows the details of the successful timing observations from the various telescopes.

The original set of detections at 1400 MHz taken at Parkes between 2001 and 2004 could not be phase connected with our timing solution and are not included here. Additional timing observations in the future may be useful for phase connecting these older Parkes data, but the timing jitter and the systematics present in the TOAs may preclude this (see discussion below).

3. TIMING RESULTS

Timing data from the three telescopes spanning a total of 522 days were phase connected using the TEMPO software package.[16] The BTX binary model (D. Nice, unpublished) was used. This is a modification of the BT binary model (Blandford & Teukolsky 1976) that allows for multiple derivatives of the orbital frequency to be included, as is necessary for PSR J1723−2837. We used the UTC(NIST) time standard and the JPL DE405 solar system ephemeris for barycentric corrections. The TOA uncertainties were adjusted for each observing setup by a multiplicative factor (EFAC in TEMPO) to account for underestimated values produced in the generation of the TOAs. Specifically, TOAs from each observing setup were separately fit to the timing model such that the chosen multiplicative factor produced a reduced χ^2 close to unity. The combined data set was then fit with these separate factors in place for each subset. The TOAs were weighted in the comprehensive fit according to their uncertainties. Systematics present in the residuals required the inclusion of orbital frequency derivatives up to the third derivative to whiten the residuals.

The timing solution is presented in Table 2, and the quoted uncertainties in the timing parameters are twice the formal TEMPO uncertainties. This is common practice when the uncertainties have been increased by EFAC. The multiple

[16] http://tempo.sourceforge.net

Table 2
Timing Parameters for PSR J1723−2837

Parameter	Value
Measured Quantities	
Right ascension (J2000)	17:23:23.1856(8)
Declination (J2000)	−28:37:57.17(11)
Spin frequency, f (s^{-1})	538.870683485(3)
Frequency derivative, $\dot{f}$ (s^{-2})	$-2.19(12) \times 10^{-15}$
Dispersion measure, DM (pc cm^{-3})	19.688(13)
Timing epoch (MJD)	55667
Time of ascending node, T_{asc} (MJD)	55425.320466(2)
Projected semi-major axis, x (s)[a]	1.225807(9)
Orbital frequency, f_b (s^{-1})	$1.88062856(2) \times 10^{-5}$
Orbital frequency derivative, $\dot{f}_b$ (s^{-2})	$1.24(4) \times 10^{-18}$
Orbital frequency second derivative, $\ddot{f}_b$ (s^{-3})	$-2.6(3) \times 10^{-26}$
Orbital frequency third derivative, $\dddot{f}_b$ (s^{-4})	$-6.2(6) \times 10^{-33}$
1400 MHz flux density, S_{1400} (mJy)[b]	1.1
2000 MHz flux density, S_{2000} (mJy)[b]	0.2
W_{50} at 1520 MHz (ms)[c]	0.20
W_{50} at 2000 MHz (ms)[c]	0.27
W_{50} at 3100 MHz (ms)[c]	0.21
Derived Quantities	
Spin period, P (ms)	1.855732795728(8)
Spin period derivative, $\dot{P}$	$7.5(4) \times 10^{-21}$
Orbital period, P_b (d)	0.615436473(8)
Orbital period derivative, $\dot{P}_b$	$-3.50(12) \times 10^{-9}$
Companion mass range ($M_\odot$)[d]	0.4–0.7
Orbital inclination angle range (degrees)[d]	30–41
Galactic longitude, l (deg)	357.6
Galactic latitude, b (deg)	+4.3
Surface magnetic field, B (G)[e]	1.2×10^8
Spin-down luminosity, $\dot{E}$ (erg s^{-1})[e]	4.6×10^{34}
Characteristic age, τ_c (Gyr)[e]	3.9
Distance, d (kpc)[f]	0.75(10)
Distance from Galactic plane, $\lvert z\rvert = d \sin \lvert b\rvert$, (kpc)	0.06
1400 MHz radio luminosity, $L_{1400} = S_{1400} d^2$ (mJy kpc^2)	0.6
Observational Parameters	
Discovery observation MJD	51973
Phase-connected TOA range (MJD)	55102–55623
Timing span (d)	522
Weighted rms post-fit residual (μs)	20.9

Notes. Figures in parentheses are uncertainties in the last digit quoted and are twice the formal errors from the TEMPO timing solution.
[a] $x = a \sin i / c$ where a is the semi-major axis and i is the orbital inclination angle.
[b] Flux density measured away from eclipse. The value was estimated using the radiometer equation applied to the original survey discovery observation (for S_{1400}) and the GBT observation shown in Figure 8 (for S_{2000}).
[c] Width at which the measured pulse reaches 50% of its peak value. See Figure 8.
[d] Assumes a pulsar mass between 1.4 and 2.0 $M_\odot$.
[e] $B = 3.2 \times 10^{19} (P\dot{P})^{1/2}$; $\dot{E} = 4\pi^2 I \dot{P} / P^3$, with an assumed moment of inertia $I = 10^{45}$ g cm^2; $\tau_c = P/2\dot{P}$. These parameters depend on $\dot{P}$ which has not been corrected for the Shklovskii effect.
[f] Estimated from the NE2001 DM-distance model of Cordes & Lazio (2002). The uncertainty in the distance was also obtained from this model.

observing frequencies allowed us to fit for a dispersion measure (DM) of 19.688(13) pc cm^{-3}. This indicates a relatively small distance to the pulsar ($d \sim 0.75$ kpc), according to the NE2001 DM-distance model of Cordes & Lazio (2002). Figure 1 shows the timing residuals after fitting the TOAs to the timing model. The residuals are shown as a function of both date and orbital phase, with a weighted rms of the residuals of 21 μs.

The timing-derived period derivative is $\dot{P} = 7.5(4) \times 10^{-21}$. This not only includes Galactic acceleration and rotation contributions, but also an undetermined contribution from the Shklovskii effect (Shklovskii 1970), which is caused by the pulsar's transverse motion. Following the analysis of Nice & Taylor (1995), we find that the acceleration and rotation contributions to $\dot{P}$ are negligible (<2% combined). The Shklovskii effect, however, may be significant given the small distance to the pulsar. The measured $\dot{P}$ is highly sensitive to the transverse speed: a speed of 170 km s^{-1} at the pulsar's estimated distance of 0.75 kpc would produce a Shklovskii term that would entirely account for the measured $\dot{P}$. This provides an upper limit of ∼170 km s^{-1} beyond which the Shklovskii $\dot{P}$ would exceed the measured $\dot{P}$. Including a fit for proper motion in the timing

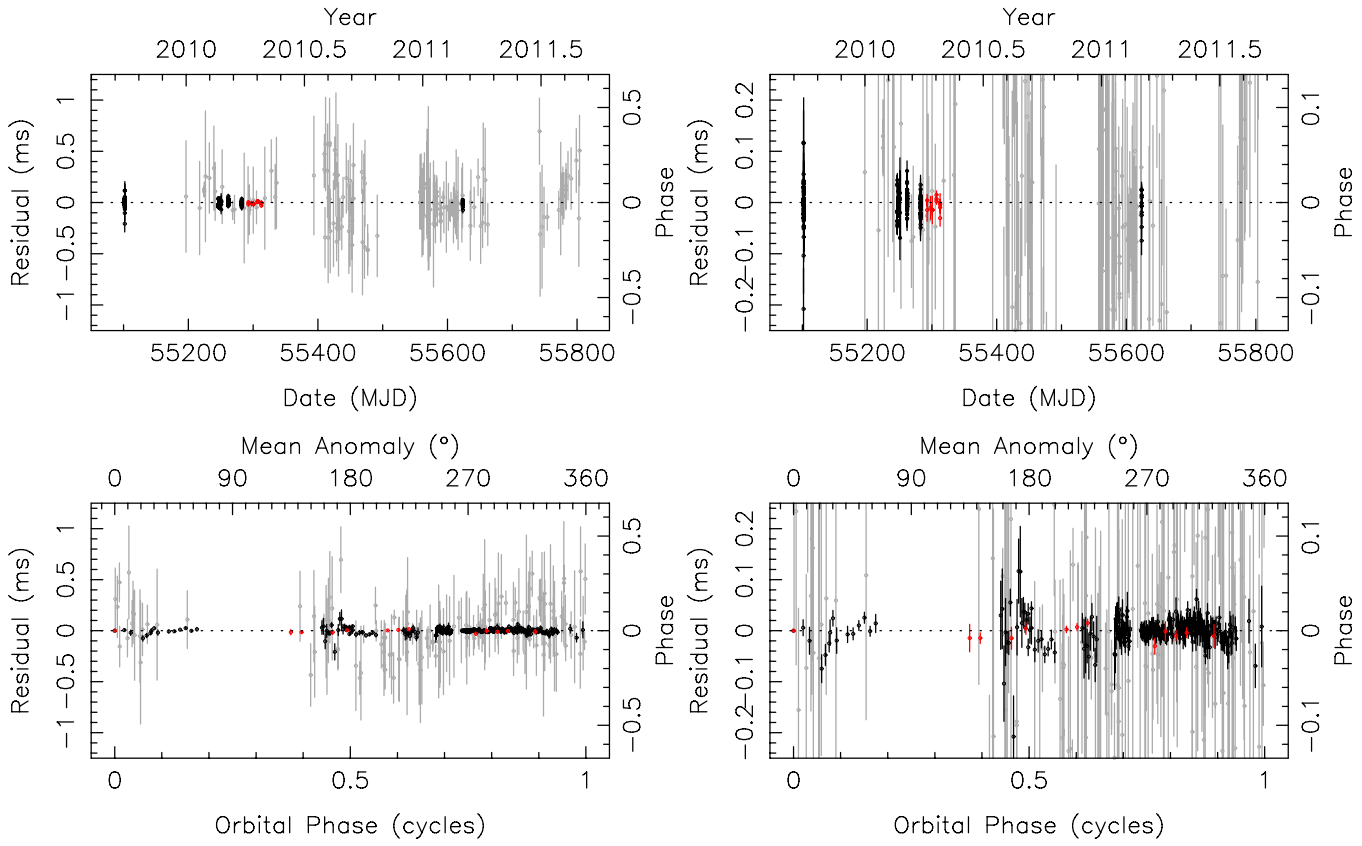

Figure 1. Timing residuals for PSR J1723−2837 shown as a function of date (top) and orbital phase (bottom). The TOAs from the three different telescopes used are color coded (black for 2000 MHz GBT data; light gray for 1520 MHz Jodrell Bank data; red for 1369 and 3100 MHz Parkes data). The plots on the right show the same data as the plots on the left, but on a smaller scale so that the higher-precision GBT and Parkes TOAs can more easily be seen. The timing solution is presented in Table 2 and has an rms residual of 21 μs. No detections were made for ∼15% of the orbit at phases near 0.25, despite some attempts to observe the pulsar during these phases. This is consistent with eclipsing by an extended companion envelope. The TOA uncertainties for each data subset were scaled to produce a reduced χ^2 close to one for that subset in order to account for the additional uncertainty introduced by both instrumental and astrophysical sources. Several higher-order orbital frequency derivatives were included in the timing solution to whiten the residuals.

(A color version of this figure is available in the online journal.)

solution is unable to further constrain this upper limit owing to the relatively large residuals in the solution and the limited timing span (<2 yr; see Table 2).

The spin-down power of the pulsar determined using the measured (uncorrected) $\dot{P}$ is $\dot{E} = 4.6 \times 10^{34}$ erg s^{-1} ($\dot{E} \equiv 4\pi^2 I \dot{P} P^{-3}$, where I is an assumed neutron star moment of inertia of 10^{45} g cm^2). The $\dot{E}$ strongly affects the pulsar's interaction with its companion and can produce ablation of the companion which obscures the pulsar's signal. The measured $\dot{E}$ is typical of those measured for MSPs listed in the ATNF Pulsar Catalogue, which range from $\sim 10^{32}$ to $\sim 10^{36}$ erg s^{-1}, and it is close to the values of $\dot{E}$ measured for known Galactic redbacks, all of which have $\dot{E} \sim 10^{34}$ erg s^{-1} (see Deller et al. 2012 and Table 1 of Roberts 2013). However, none of these $\dot{E}$ measurements for the redbacks (with the exception of PSR J1023+0038) have been corrected for the Shklovskii effect, so the intrinsic $\dot{E}$ for these pulsars could be much smaller. The pulsar's characteristic age is $\tau_c \equiv P/2\dot{P} > 3.9$ Gyr, and the estimated surface magnetic field is $B \equiv (3.2 \times 10^{19})(P\dot{P})^{1/2}$ G $< 1.2 \times 10^8$ G. Again, these have not been corrected for the Shklovskii effect, so lower and upper limits are quoted here. These values are consistent with the values expected for a recycled MSP.

PSR J1723−2837 follows an almost circular orbit, and the orbital eccentricity is too small to be measured in our fit when the orbital period derivatives are included in the timing solution. The large orbital period derivative (see Table 2) is a signature of a strong tidal effect between the neutron star and an extended, mass-losing companion (Lazaridis et al. 2011). In addition, the pulsar is eclipsed for a significant portion of its orbit (∼15%; see Figure 1). The eclipsing occurs at orbital phases near 0.25, when the pulsar is behind its companion. These features suggest that the companion is a non-degenerate, extended star, which we confirm below.

PSR J1723−2837 exhibits significant flux variability on the time scale of minutes. Figure 2 shows detections at 2000 MHz with the GBT which illustrate this variability. One possible contribution to this is diffractive scintillation, which may be significant given the pulsar's small DM. Dynamic spectra constructed using both the Parkes 1.4 GHz discovery observation and a bright 2 GHz GBT timing observation have decorrelation bandwidths of 12 MHz and 100 MHz, respectively, and decorrelation times of 18 minutes and 30 minutes. These are all within a factor of two of the values predicted by the NE2001 model (Cordes & Lazio 2002). The decorrelation times are similar to the observed variability time-scales, but the decorrelation bandwidths are much smaller in each case than the observing bandwidths used. This suggests that eclipsing or obscuration by material from the companion (and not scintillation) is the dominant factor in the variability.

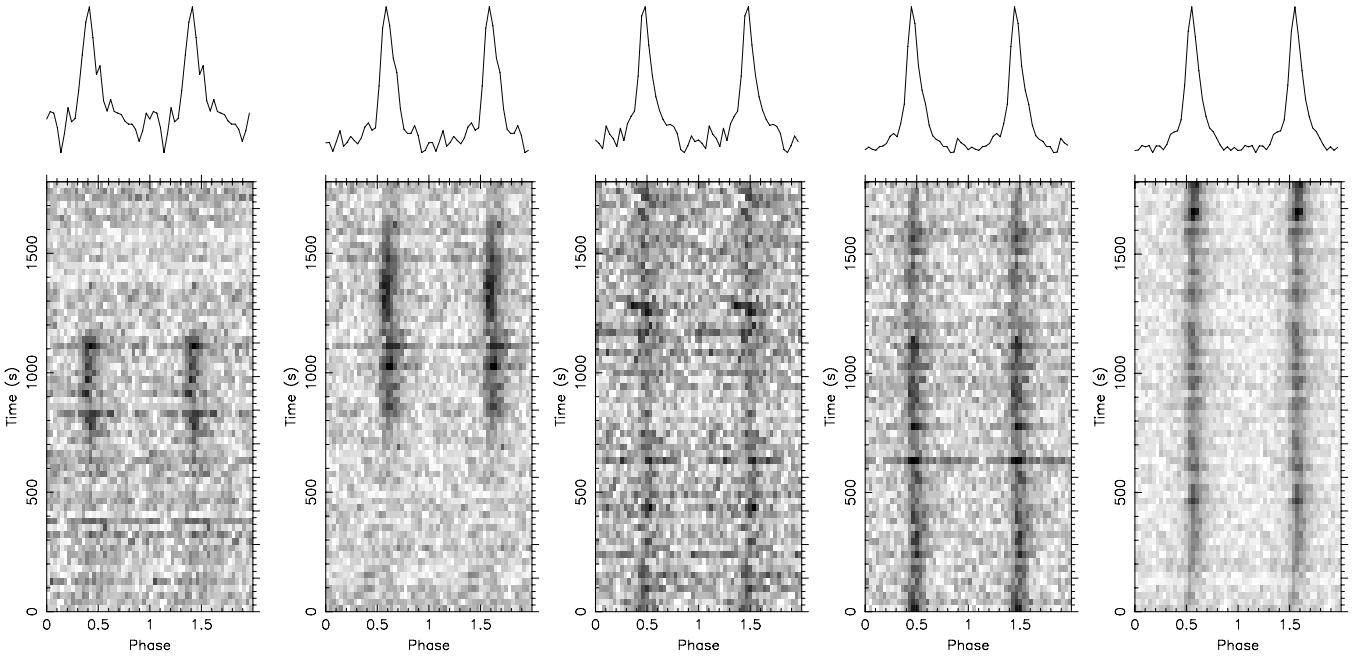

Figure 2. Time-resolved folded pulse profiles of PSR J1723−2837 taken at 2000 MHz with the GBT. The time-integrated profile is shown above each time-resolved profile plot. Each observation had an integration time of 30 minutes. The flux variability is evident in these profiles and is likely dominated by obscuration by material within the system and not diffractive interstellar scintillation.

Table 3
Photometry of the Optical Companion of PSR J1723−2837

Band	Central Wavelength (Å)	Measured Magnitude	Survey/Telescope[a] Source	Observation Date	Magnitude[b] System
UVW2	1928	22.63 ± 0.23	*Swift*	2010 Mar 5	AB
u	3450	18.53 ± 0.05	*Swift*	2010 Mar 5	AB
B	4380	16.94 ± 0.02	WIYN	2012 May 31	Vega
V	5450	15.78 ± 0.04	WIYN	2012 May 31	Vega
R	6410	15.15 ± 0.02	WIYN	2012 May 31	Vega
I	7980	14.42 ± 0.07	WIYN	2012 May 31	Vega
Z	8780	14.25 ± 0.01	VVV	2012 May 31	Vega
Y	10210	14.07 ± 0.01	VVV	2011 Aug 5	Vega
J	12540	13.71 ± 0.01	VVV	2011 Aug 5	Vega
J	12350	13.65 ± 0.05	2MASS	1998 Jul 12	Vega
H	16460	13.27 ± 0.01	VVV	2010 Aug 3	Vega
H	16620	13.21 ± 0.02	2MASS	1998 Jul 12	Vega
K_s	21490	13.07 ± 0.01	VVV	2011 Sep 22	Vega
K_s	21590	13.07 ± 0.02	2MASS	1998 Jul 12	Vega

Notes.
[a] Survey or telescope origin of the measurement. 2MASS is the Two Micron All-Sky Survey (Skrutskie et al. 2006). VVV is the VISTA Variables in the Via Lactea Survey (Minniti et al. 2010).
[b] Measurements were in either the AB or Vega magnitude system.

4. PHOTOMETRIC IDENTIFICATION AND SPECTROSCOPIC STUDY OF THE COMPANION

4.1. Infrared, Optical, and Ultraviolet Photometry

We identified the companion to PSR J1723−2837 in the infrared, optical, and ultraviolet bands using photometry using both archival data and new observations. This is outlined below and summarized in Table 3.

4.1.1. Archival Optical and Near-Infrared Data

The timing position of PSR J1723−2837 places it within 0.″06 of the moderately bright Two Micron All-Sky Survey (2MASS; Skrutskie et al. 2006) star J17232318−2837571. The number density of stars brighter than this is 0.004 arcsec^{-2}, so there is a low probability of coincidence and the association is secure. The 2MASS photometry is presented in Table 3. Apart from 2MASS, the source was clearly visible in the Digitized Sky Survey (DSS). However, because of the poor quality of the DSS photometry we rely on our new optical measurements, which are discussed below. The star was also detected in the Deep Near Infrared Survey of the Southern Sky (Epchtein et al. 1999) with magnitudes Gunn-$i = 14.70 \pm 0.05$, $J = 13.97 \pm 0.11$, and $K_s = 13.44 \pm 0.20$. The J and K_s magnitudes are about 0.3–0.4 mag fainter than those from 2MASS. While this might indicate variability, the crowded fields might also have affected

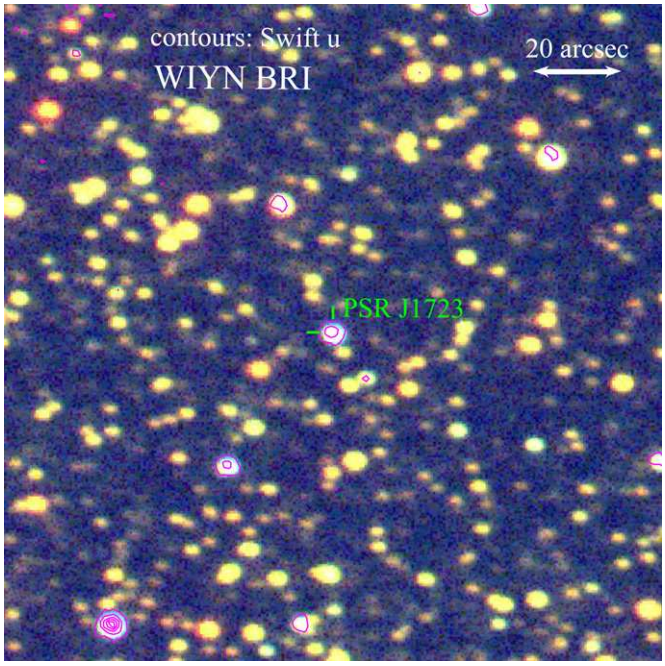

Figure 3. Three-color composite image of the field of PSR J1723−2837 created from the WIYN 0.9 m data in the *B*, *R*, and *I* filters. Contours are from *Swift* *u*-band data. The image is 150″ across, and north is up with east to the left. The position of PSR J1723−2837 is indicated by the tick marks. The bar in the upper right of the image is 20″ in length.

(A color version of this figure is available in the online journal.)

the automated photometry of one or both surveys. Since the 2MASS photometry is very close to other near-IR photometry (see below and Table 3) we use those values, but urge caution in making detailed inferences based on the precise numbers chosen.

4.1.2. WIYN Optical Observations

We observed the companion of PSR J1723−2837 with the S2KB camera on the Wisconsin–Indiana–Yale–NOAO (WIYN) 0.9 m telescope on the night of 2012 May 31 under photometric conditions. We took two 300 s exposures of the field in the *BVRI* filters, along with two 180 s exposures of the Stetson (2000) field L111. Reduction followed standard procedures in IRAF. We determined photometric zero-points from 20–150 stars in the L111 field, depending on the band, with typical zero-point uncertainties of 0.02 mag. Our final photometry is given in Table 3. We also show a three-color (*BRI*) composite image of the field in Figure 3, with contours from the *Swift* *u*-band observation overlaid (see *Swift* observations below). It is apparent that the optical companion to PSR J1723−2837 is brighter and bluer than most of the field stars. We quantify this in the spectral energy distribution in Section 4.4.

4.1.3. Swift Ultraviolet Observations

An observation of the field with the *Swift* satellite from 2010 March 5 shows a bright source at the radio position in the data from the Ultraviolet and Optical Telescope (UVOT; Roming et al. 2005). In the *u* filter there was a single 765 s exposure, while in the UVW2 filter there were 13 exposures totaling 5577 s; both bands used 2 × 2 pixel binning. We determined summed photometry from these data using *Swift* data-reduction tools. We summed the UVW2 integrations and measured the summed magnitude with a source radius of 5″ centered on the radio position and a background region 25″ in radius centered near the pulsar, but not including any visible sources. The final detection significances in the summed images were 23.1σ (*u* filter) and 4.8σ (UVW2 filter), but our photometry includes the suggested systematic uncertainties (0.02 mag and 0.03 mag, respectively) in addition to the statistical uncertainty. The details of the photometry are presented in Table 3.

4.1.4. VVV Infrared Data

Finally, we assembled photometry from the VISTA Variables in the Via Lactea Survey (VVV; Minniti et al. 2010) Data Release 1. Although this is a time-domain survey, we only had access to a single epoch of data for each filter ($ZYJHK_s$). We followed the recommended procedure to extract calibrated photometry from the data,[17] using the recommended photometric zero-point uncertainty of 0.01 mag. We note that while the VVV photometry has been calibrated with respect to 2MASS, Saito et al. (2012) gives slightly different effective wavelengths than Cohen et al. (2003). Our final photometry is given in Table 3.

4.2. Optical Spectroscopy with Palomar and WIYN

After the photometric identification of the coincident star, we obtained two epochs of low-resolution spectroscopy with two telescopes. We observed the companion of PSR J1723−2837 with the Double Spectrograph (DBSP) on the 5 m Palomar (Hale) telescope. We obtained two 300 s exposures on 2012 March 20 and 21. The blue side used the 600 line mm^{-1} grating (1.07 Å pixel^{-1}, covering 3700–5500 Å) while the red side used the 316 line mm^{-1} grating (1.53 Å pixel^{-1}, covering 5500–10000 Å, although beyond 7000 Å fringing and uncertain telluric corrections make the data not very useful), with the 5500 Å dichroic separating the sides and a 1″ slit. Reduction followed standard procedures in IRAF. We determined the wavelength solution using Fe/Ar arc lines for the blue side (61 lines with an rms residual of 0.22 Å) and He/Ne/Ar lines for the red side (27 lines with an rms residual of 0.07 Å). Rough flux calibration was relative to the spectrophotometric standard star BD+28 4211.

We also observed the companion of PSR J1723−2837 for two 300 s exposures on 2012 March 21 and 22 using the Bench Spectrograph with the Sparsepak fiber bundle (Bershady et al. 2004) on the 3.5 m WIYN telescope. These observations used the Red camera and the 600 line mm^{-1} grating, centered at a wavelength of 5200 Å, with the CCD binned substantially (4 pixels in the spatial dimension and 3 in the spectral dimension). Reduction followed standard procedures[18] in IRAF. We determined a wavelength solution using 49 lines from the Cu/Ar lamp, with an rms residual of 0.7 Å. The background was subtracted using a nearby fiber that was determined not to cover a star (as identified from the images discussed above). The wavelength coverage was 3800–6630 Å with a scale of 2.1 Å pixel^{-1}. Rough flux calibration was done with an observation of the spectrophotometric standard HZ44.

Table 4 summarizes these two sets of spectral observations. For both sets the pulsar was at an airmass of between 2.0 and 2.2, so the flux calibration and telluric line removal in the red may not be very reliable.

4.3. Spectral Type and Radial Velocities

We used our spectra to try to establish a spectral type for the optical companion. We show one of the Palomar spectra in

[17] See http://www.eso.org/sci/observing/phase3/data_releases/vvv_dr1.html.
[18] See http://www.astro.wisc.edu/~cigan/reducing/reducing.html.

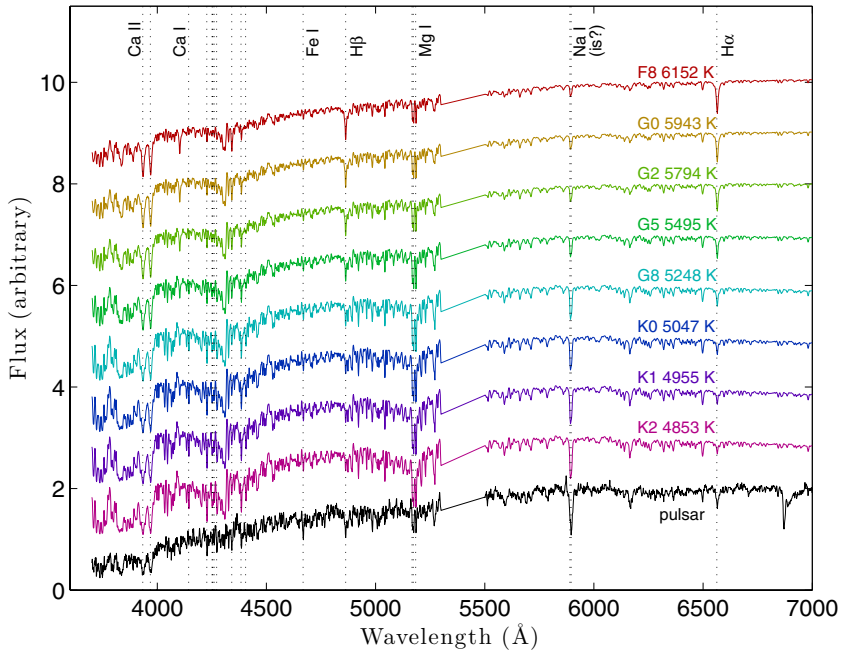

Figure 4. Spectrum of the optical companion to PSR J1723−2837 from the 2012 March 20 Palomar observation (bottom), along with main-sequence model spectra from Munari et al. (2005). The models go (top to bottom) from F8 (effective temperature 6150 K) to K2 (4850 K), as labeled. The model spectra have been convolved to match the resolution of the data and have been multiplied by a linear function to match the continuum slope of the data. Selected absorption lines are labeled, with the possible interstellar contribution to the Na I line indicated.

(A color version of this figure is available in the online journal.)

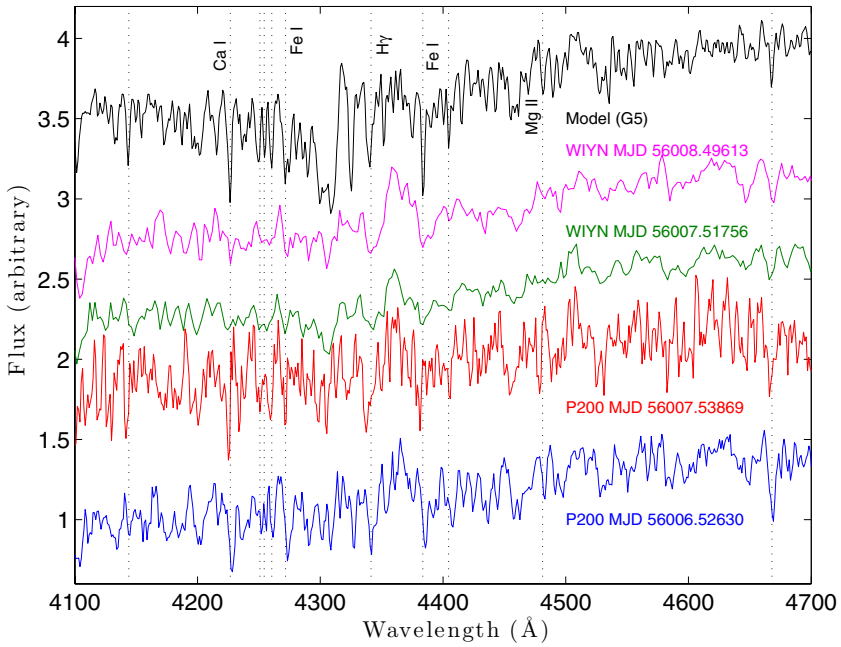

Figure 5. G5 model spectrum is shown (at the top) along with the measured spectra of the optical companion to PSR J1723−2837 from the Palomar and WIYN observations (labeled). Selected absorption lines are also labeled. The velocity shift between the two Palomar spectra is readily visible (e.g., in the Ca I λ4226 line), although similar shifts are also seen in the WIYN spectra. The MJD values shown have not been corrected to the solar system barycenter. The measured Doppler velocities from these spectra are presented in Table 4.

(A color version of this figure is available in the online journal.)

Figure 4, along with model spectra of types F8-K2 (see also Figure 5). A comparison of our spectra to these model spectra as well as to the Gray spectral atlas[19] indicates that the spectral type of the companion seems to be somewhere around FGK, although the precise type is hard to pin down. The Na I λ5891 line is strong, as in a late G or early K star, but some of this could be from interstellar absorption; a full sampling of radial velocities should be able to disentangle this. This appears to agree with the modest depth of the Ca II H and K lines. Cr I λ5254 is about equal in strength to Fe I λ4250 and λ4260, which would place the companion somewhere near K0. Fe I λ4325 is roughly equal in depth to Hγ, which would put it somewhere

[19] See http://ned.ipac.caltech.edu/level5/Gray/frames.html.

Table 4
Doppler Spectroscopy of the Optical Companion of PSR J1723−2837

Telescope	Date (UT Time)	MJD	Velocity (km s^{-1})	Orbital Phase
Palomar	2012 Mar 20 (12:41)	56006.52852	+145 ± 5	0.39
WIYN	2012 Mar 21 (12:28)	56007.51978	−52 ± 25	1.00
Palomar	2012 Mar 21 (12:59)	56007.54095	−116 ± 10	0.03
WIYN	2012 Mar 22 (11:57)	56008.49839	+127 ± 15	0.59

Notes. Times and velocities have been converted to the solar system barycenter. Times correspond to the middle of the 300 s exposure in each case.

between G5 and K0. However, the molecular *G*-band is rather weak, more similar to an earlier G star. Other lines like Fe I λ4668 also appear stronger in the observed spectrum than in all of the models (other Fe I lines are similarly strong). The Mg I lines near 5180 Å appear modest in strength, but the MgH complex that overlaps with those lines in later-type stars is not apparent. Overall, our spectral data indicate that the optical companion to PSR J1723−2837 has an effective temperature of 5000–6000 K and a surface gravity that is reasonably consistent with that of a main-sequence star. Beyond that we cannot make firm conclusions from these spectra. It could be that the metallicity of the companion is significantly different from the templates or that some other effect is causing variations in individual lines (e.g., rotation or an anomalously low surface gravity). The pulsar's wind also has a significant heating effect on the companion's atmosphere, which may modify the apparent spectral type and would contribute to its uncertainty.

We then determined the radial velocities of the individual observations. We did this by fitting each spectrum to a shifted and convolved template of a type G5 star. For the Palomar data, we verified that the sky lines at 4358 Å, 5460 Å, and 5577 Å were consistent between the two observations. For the WIYN data, the 4358 Å sky line was used to establish the velocity reference, and we used the data between 3880 Å and 5000 Å (where we had good sensitivity in all observations). We determined velocities for both Palomar observations and for both WIYN observations and corrected the observed velocities to the solar system barycenter. These measurements are presented in Table 4 and are shown in Figure 6. A region of each spectrum is shown in Figure 5, where the shift between the Palomar observations is readily apparent. The lower resolution and signal-to-noise ratio of the WIYN observations make the shift harder to discern, but it is also present.

The Palomar and WIYN observations from 2012 March 21 were taken 30 minutes apart from each other and are at almost the same orbital phase. While the velocities are not formally consistent with each other within the uncertainties (see Table 4), the uncertainties of the WIYN observations may be somewhat underestimated, and the disagreement is considerably less than the change between the two Palomar observations. Moreover, the measured velocities are consistent with those expected at the various orbital phases. This is additional evidence supporting the association between the star and PSR J1723−2837. Figure 6 shows a sinusoidal fit (with fixed phase, period, and offset) to the four measured velocities. The best-fit velocity amplitude is 143 km s^{-1}, with an uncertainty estimated to be ±20 km s^{-1} owing to the meager sampling and inhomogeneous data. Using this measured velocity amplitude and the projected semi-major axis for the pulsar (Table 2), we derive a mass ratio of 3.3 ± 0.5, giving a companion mass range of 0.4 to 0.7 $M_\odot$ and an orbital

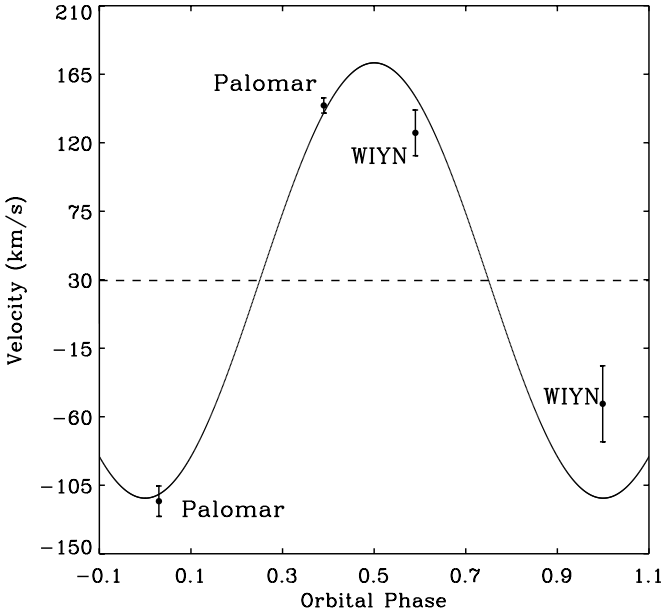

Figure 6. Measured Doppler velocities from the Palomar and WIYN spectra (see Table 4). The velocities have been corrected to the solar system barycenter. Overlaid is the best-fit sinusoid with a fixed phase, period, and offset (taken from the barycenter correction), but with an unknown amplitude. The best fit velocity amplitude is 143 km s^{-1} with an estimated uncertainty of ±20 km s^{-1}. For an assumed pulsar mass range of 1.4–2.0 $M_\odot$, the corresponding companion mass range is 0.4–0.7 $M_\odot$, and the orbital inclination angle is between 30° and 41°.

inclination angle range of 30° to 41° for an assumed pulsar mass of between 1.4 and 2.0 $M_\odot$. This pulsar mass range reflects the fact that some MSPs have measured masses above the canonical value of 1.4 $M_\odot$ (Demorest et al. 2010; Freire et al. 2011; Antoniadis et al. 2013). The inhomogeneity of the data and the small number of observations preclude a more precise radial-velocity measurement, but further observations will be able to easily determine this number to high precision and may allow for an independent estimate of the pulsar mass if the inclination angle can be independently constrained via light curve modeling (e.g., van Kerkwijk et al. 2011; Romani et al. 2012).

4.4. Spectral Energy Distribution

With the range of spectral types established in Section 4.3 and Figure 4, we can see whether the magnitudes from photometry are consistent with the spectral values, and we can use these magnitudes to determine the normalization and extinction. Using the best photometry available (the *Swift u*-band, WIYN, and VVV data), we fitted reddened models from Kurucz (1993, since the models from Munari et al. 2005 did not extend into the near-infrared). We obtained reasonable fits for models consistent with our spectral inferences: effective temperatures between 4800 K and 6000 K all fit, with the extinction varying between $A_V = 0.2$ mag to 1.7 mag over that range. We did have to assume a modest (5%) systematic uncertainty, but given the variations in the assumed filter transmission curves and the lack of color terms in our photometric calibration, this was reasonable. The best fit was for an effective temperature of 5500 K (spectral type G5) and an extinction of $A_V = 1.2$ mag, as shown in Figure 7, although the exact fit varies a little if we change the systematic uncertainties. This temperature is somewhat higher than the temperature expected from the heating of the companion from the pulsar wind if 100% of the measured $\dot{P}$ were intrinsic to

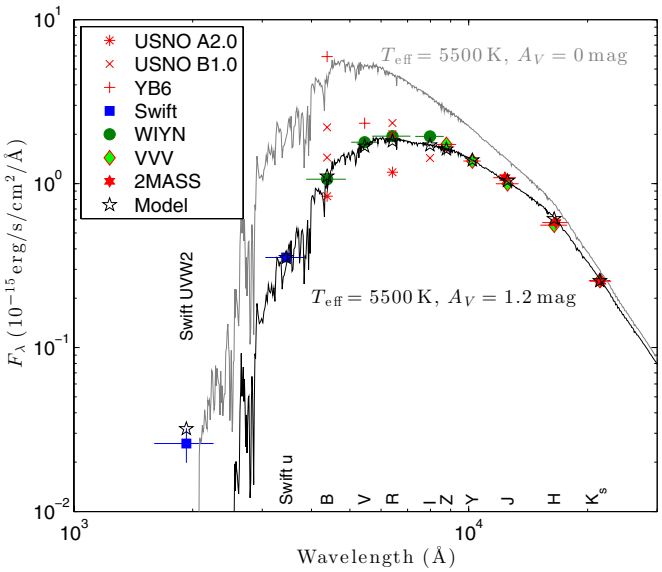

Figure 7. Spectral energy distribution of the optical companion to PSR J1723−2837. The data from *Swift* (squares), WIYN (circles), VVV (diamonds), and 2MASS (stars) surveys are plotted along with the best-fit spectral model from Kurucz (1993). The black trace is a 5500 K (roughly G5) model including an extinction of $A_V = 1.2$ mag, while the gray trace is without extinction; the black stars represent the black trace model convolved with the filter response curves. We also plot data from the USNO-A2.0, USNO-B1.0, and YB6 catalogs (Monet et al. 1998, 2003) based on the Naval Observatory Merged Astrometric Dataset (NOMAD).

(A color version of this figure is available in the online journal.)

the pulsar, if the wind were isotropic, and if the companion had a 15% absorption efficiency factor (see, e.g., Breton et al. 2013). The expected temperature range from this would be 3100–3600 K for the inclination angle range 30° to 41°. While we did not use the 2MASS or *Swift* UVW2 data for the fitting, our model also fits these data well (the 2MASS data are largely consistent with the VVV data). We also see that the scanned-plate data from the USNO-A2.0, USNO-B1.0, and YB6 catalogs (Monet et al. 1998, 2003) are plausibly matched by the data. There is some scatter, and this may arise from difficulties in converting the USNO photometry to fluxes, or it could indicate variability in the photometry across the orbit, as in the case of PSR J1023+0038 (Wang et al. 2009). Based on the observed K_s-band flux, we estimate a normalization of 1.2 $R_\odot$ kpc^{-1}.

5. DISCUSSION

Figure 8 shows integrated pulse profiles for PSR J1723−2837 at 1520, 2000, and 3100 MHz that were taken at orbital phases far from eclipse. There is evidence of asymmetry in all of the profiles, which could indicate interstellar scattering. However, several pieces of evidence argue against this. First, the NE2001 model indicates that the scattering time-scale from the interstellar medium in this direction for a DM of 20 pc cm^{-3} is negligible ($\lesssim 10^{-7}$ s at 1 GHz). Second, the scatter-broadening time would be significantly larger at 1520 MHz than at 3100 MHz (by a factor of ∼11 for a power-law frequency dependence of $\nu^{-3.4}$; Löhmer et al. 2001). As seen in Figure 8, the profiles at all frequencies appear to have a similar tail length, which would not be expected from scattering. We conclude that the asymmetry in the pulse profiles is intrinsic to the beam shape and that the profile does not evolve significantly between these frequencies.

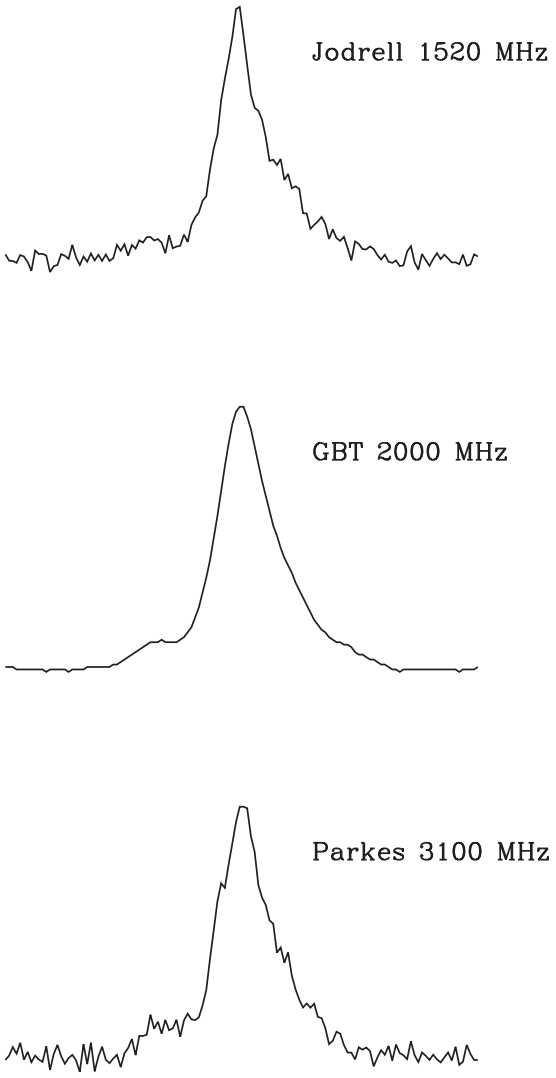

Figure 8. Pulse profiles for PSR J1723−2837 at 1520 MHz from Jodrell Bank (top), 2000 MHz from the GBT (middle), and 3100 MHz from Parkes (bottom). Each profile has 128 bins, and the full profile is shown in each case. The profiles were constructed from observations of 40, 62, and 60 minutes, respectively. In all cases the observations were taken at orbital phases far from the eclipsing region. The similarity between the profiles indicates that the trailing extension of the profile is not due to interstellar scattering.

It is clear that eclipsing by the companion introduces a large flux variability throughout the orbit at all observed frequencies, and this is responsible for some of our non-detections at 1400 MHz with Parkes. Figure 1 shows the timing residuals as a function of orbital phase. There are no detections for ∼15% of the orbit, centered near a phase of 0.25, when the pulsar is behind the companion (at inferior conjunction). This is partially due to the scheduling of most of the observations to occur away from the eclipse phase range in order to maximize the likelihood of detection. However, some of the 2000 MHz GBT observations were taken at orbital phases between 0.5 and 0.6, well away from the eclipse phases near 0.25, and the pulsar was not detected in these cases. This suggests that eclipsing may not be the only reason for the non-detections; for instance, the pulsar might be shrouded at times by gas or an extended companion wind that is being driven by the pulsar (see below). PSR J1723−2837 is similar in this sense to the GC pulsars PSR J0024−7204W (47 Tuc W) and PSR J1740−5340. PSR J0024−7204W has a low-mass companion and exhibits eclipses lasting for about

Table 5
Galactic Redbacks

Pulsar	$\dot{E}_{34}/d^2_{\rm kpc}$	Reference	*Fermi* Detected?	γ-ray Efficiency[a]
J1723−2837	8.2	This paper	No	<0.007
J2129−0429	4.8	Hessels et al. (2011)	Yes	0.02
J1023+0038	2.3	Tam et al. (2010)	Yes	0.03
J1628−3205	1.3	Ray et al. (2012)	Yes	0.11
J1816+4510[b]	0.9	Kaplan et al. (2012)	Yes	0.20
J2215+5135	0.7	Hessels et al. (2011)	Yes	0.17

Notes. Entries are rank-ordered by $\dot{E}_{34}/d^2_{\rm kpc}$, an indicator of detectability at high energies. $\dot{E}_{34} = \dot{E}/10^{34}$ erg s^{-1} and $d_{\rm kpc}$ is the distance in kiloparsecs. $\dot{E}$ values should be considered upper limits in all cases (except for J1023+0038) since the measured $\dot{P}$ has not been corrected for proper motion. Values of $\dot{E}$ and d for all pulsars (except for PSR J1723−2837 and J1023+0038) were taken from Table 1 of Roberts (2013).
[a] Assumes that the measured $\dot{P}$ is entirely intrinsic to the pulsar.
[b] The companion to PSR J1816+4510 appears to be a white-dwarf-like object with substantial metals (Kaplan et al. 2013) and is therefore unlike the other redbacks listed.

half of the orbital period (Camilo et al. 2000; Edmonds et al. 2002). PSR J1740−5340 is an eclipsing pulsar with a bright optical companion that fills its Roche lobe (D'Amico et al. 2001; Ferraro et al. 2001). There are other examples of such pulsars in GCs: PSR J1701−3006B in M62 (Possenti et al. 2003), which has a companion optically identified by Cocozza et al. (2008), and PSRs J1824−2452H and J1824−2452I in M28 (Pallanca et al. 2010; Papitto et al. 2013).

The sparse orbital coverage of the available photometric data does not allow us to constrain the degree of tidal distortion of the companion star. However, the similarity of PSR J1723−2837 to both PSR J1023+0038 (Archibald et al. 2009) and PSR J1740−5340 (Ferraro et al. 2001) suggests that the companion could be a star nearly filling its Roche lobe. For an orbital geometry using reference masses of 0.43 and 1.4 $M_\odot$ for the companion and the pulsar, respectively, the photometric data imply a distance of 0.77 kpc for the star. This nicely agrees with the 0.75 kpc distance estimated for the pulsar from the DM.

For a pulsar mass range 1.4–2.0 $M_\odot$, the corresponding radius for a Roche-lobe filling companion star is $\sim$1 $R_\odot$ (e.g., Breton et al. 2013). As expected, this radius is considerably larger than the radius of a star with the mass of the companion, suggesting substantial bloating of the companion, as is seen in the J1023+0038 and J1740−5340 systems. This radius would give an eclipse fraction of $\sim$9% of the orbit if seen edge-on, in contrast to the observed eclipse fraction of $\sim$15%, which corresponds to a eclipsing radius of $\sim$1.7 $R_\odot$. This eclipsing radius becomes even larger when the inclination angle is taken into account. This is an indication that the extended eclipse range is likely caused by a plasma wind or a cloud of outflowing matter released from the companion which overflows the Roche lobe and thus must be continuously replenished.

The features of PSR J1723−2837 suggest that it is a member of the growing class of redback systems. Redbacks are binary millisecond radio pulsars with short-period, circularized orbits and with extended companions having masses of a few tenths of a solar mass (see Roberts 2013). As mentioned above, the first two objects likely belonging to this class were found about a decade ago in GCs. The first system in the Galaxy to be confirmed as a redback, PSR J1023+0038 (Archibald et al. 2009), is believed to have turned on as a radio pulsar after a recent phase in which there was an accretion disk which is no longer present in the system (Wang et al. 2009). This pulsar is thought now to be in a bi-stable state, switching between radio pulsar and LMXB phases according to the changing rate at which the companion overflows its Roche lobe, as is observed for PSR J1824−2452I (Papitto et al. 2013). All of the currently known Galactic redbacks (including PSR J1723−2837) are nearby field pulsars ($d \lesssim 3$ kpc).

Given that all Galactic redbacks discovered so far have been successfully detected as γ-ray sources with *Fermi*, it is likely that there are high-energy counterparts to PSR J1723−2837. The SIMBAD database[20] indicates that there is a cataloged *ROSAT* X-ray point source (1RXS J172323.7−283805) located 13″ from the position of PSR J1723−2837. The uncertainty in the X-ray position is given as 17″, making its position consistent with that of PSR J1723−2837. The average sky density of *ROSAT* sources in the 1RXS catalog (Voges et al. 1999) is low (less than one cataloged source per square degree), making the likelihood of a chance coincidence with the pulsar very small ($\sim 10^{-5}$). A cataloged *INTEGRAL* hard X-ray source (IGR J17233−2837) is also located only $\sim$1′ from the pulsar (Krivonos et al. 2010). This is also a likely association given the large uncertainty of the source position. In contrast, the second Fermi-LAT catalog (2FGL; Nolan et al. 2012) shows no cataloged source within one degree of PSR J1723−2837.

As discussed by Roberts (2013), there are five other redback systems with characteristics like PSR J1723−2837, all of which are Fermi-detected sources. Table 5 lists these five systems and PSR J1723−2837 ranked by $\dot{E}/d^2$, which is a measure of detectability at high-energies. $\dot{E}$ and d in this table were obtained from Table 1 of Roberts (2013), but only PSR J1023+0038 has an $\dot{E}$ that has been corrected for the Shklovskii effect and for Galactic accelerations (Deller et al. 2012). As seen in Table 5, PSR J1723−2837 ranks first among this group, indicating that high-energy emission ought to be detectable. However, a fold of *Fermi* photons with the pulsar ephemeris using a variety of energy and angle cuts shows no clear evidence of pulsed emission. This may be due in part to the large background in this part of the sky (near the Galactic plane), or PSR J1723−2837 might be sub-luminous in γ-rays owing to the orientation of the emission geometry, as described by Romani et al. (2011). The proper motion might also be near the upper limit of 170 km s^{-1} obtained from the measured $\dot{P}$ and pulsar distance. In this case, the intrinsic $\dot{P}$ and $\dot{E}$ would be much smaller than the measured values. For a proper motion of $\sim$30 km s^{-1}, which is comparable to the heliocentric radial speed of the system, the motion would contribute only a few percent of the measured $\dot{P}$ and would not significantly affect the measured values.

[20] http://simbad.u-strasbg.fr/simbad/

We can compute an upper limit to the γ-ray efficiency for PSR J1723−2837 by considering the minimum point-source fluxes for sources in the Galactic plane in the 2FGL catalog (Nolan et al. 2012). For this we assume an upper limit of 5×10^{-12} erg cm^{-2} s^{-1} on the 100 MeV–100 GeV flux. Assuming that the entire measured $\dot{P}$ is intrinsic to PSR J1723−2837, the γ-ray efficiency is 0.007, which is lower than the typical γ-ray efficiencies of ∼0.1 for MSPs. We therefore adopt this as an upper limit on the γ-ray efficiency. This value is lower than the values measured for the Galactic redbacks listed in Table 5, in some cases by more than an order of magnitude.

6. CONCLUSIONS

We present a study of the binary radio MSP PSR J1723−2837. We have determined a phase-connected timing solution for the pulsar, which is presented in Table 2. It is evident that the pulsar has a low-mass, extended companion and is in a circularized, short-period orbit. We have identified the pulsar's companion using infrared, optical, and ultraviolet photometry and spectroscopy. The mass ratio of the system measured from Doppler variations in the companion star's spectrum is 3.3 ± 0.5 (ratio of pulsar to companion mass). For an assumed pulsar mass range of 1.4–2.0 $M_\odot$, the corresponding companion mass range is 0.4 to 0.7 $M_\odot$ and the orbital inclination angle range is 30° to 41°. The best-fit spectrum for the companion indicates that it has a spectral type of G (effective temperature near 5500 K), which is consistent with the measured spectral energy distribution. The distance inferred from the observations of the companion is also consistent with the estimate obtained from the DM of the pulsar. However, the stellar radius of the companion is larger than expected, indicating that the star is likely close to filling its Roche lobe. The character of the flux variability of the pulsar, the difficulty in detecting it at low frequencies, and the eclipse fraction of ∼15% (much larger than the 9% expected from the filled Roche lobe of the companion if it were seen edge-on) also indicates that there is likely an extended region of stellar plasma responsible for the eclipsing. Measurements of the scintillation times and bandwidths indicate that diffractive scintillation does not play a dominant role in the observed flux variability. The pulsar's large spin frequency indicates that it is highly recycled (in the standard MSP production model) despite having a companion that superficially resembles a main-sequence star. These features place it in the category of Galactic redbacks (Roberts 2013). In some respects this system is similar to PSR J1023+0038 and supports the standard evolutionary picture of radio MSPs (Alpar et al. 1982). Unlike the other five Galactic redback systems discovered to date, PSR J1723−2837 is not detected as a *Fermi* source. There are several possibilities for why it is not detected. A Shklovskii correction to $\dot{E}$ from proper motion has not been accounted for, and the pulsar is located near the Galactic plane, where the background is brighter. The pulsar might also be sub-luminous in γ-rays owing to its emission orientation. PSR J1723−2837 is coincident with a *ROSAT* source and a cataloged *INTEGRAL* hard X-ray source, both of which are likely associated with the pulsar. Future radio polarimetry observations might be able to detect rotation measure variations as a function of orbital phase, which could be useful for probing the magnetized stellar wind from the companion star.

We thank David Levitan, Marsha Wolf, and Eric Hooper for assistance with the WIYN observations, and we thank Claire Gilpin and Deborah Schmidt for assistance with radio timing observations with the GBT. We also thank the anonymous referee for helpful suggestions which have improved the manuscript. The National Radio Astronomy Observatory is a facility of the National Science Foundation operated under cooperative agreement by Associated Universities, Inc. The Parkes radio telescope is part of the Australia Telescope, which is funded by the Commonwealth of Australia for operation as a National Facility managed by CSIRO. STScI is operated by the Association of Universities for Research in Astronomy, Inc., under NASA contract NAS5-26555. This research was supported in part by NRAO Student Observing Support Award GSSP09-0006. Pulsar research at UBC is supported by an NSERC Discovery Grant. P.F. gratefully acknowledges the financial support provided by the European Research Council for the ERC Starting Grant BEACON under Contract No. 279702. Part of this work was based on data products from observations made with ESO Telescopes at the La Silla or Paranal Observatories under ESO programme ID 179.B-2002, and from the WIYN Observatory, which is a joint facility of the University of Wisconsin-Madison, Indiana University, Yale University, and the National Optical Astronomy Observatories. Some of the data presented were obtained from the Multimission Archive at the Space Telescope Science Institute (MAST). Support for MAST for non-HST data is provided by the NASA Office of Space Science via grant NNX09AF08G and by other grants and contracts.

Facilities: *Swift* (UVOT), WIYN:0.9m (S2KB), WIYN (Sparsepak), Hale (DBSP), GBT, Parkes

REFERENCES

Alpar, M. A., Cheng, A. F., Ruderman, M. A., & Shaham, J. 1982, Natur, 300, 728
Antoniadis, J., Freire, P. C. C., Wex, N., et al. 2013, Sci, 340, 448
Archibald, A. M., Stairs, I. H., Ransom, S. M., et al. 2009, Sci, 324, 1411
Bershady, M. A., Andersen, D. R., Harker, J., et al. 2004, PASP, 116, 565
Blandford, R., & Teukolsky, S. A. 1976, ApJ, 205, 580
Breton, R. P., van Kerkwijk, M. H., Roberts, M. S. E., et al. 2013, ApJ, 769, 108
Camilo, F., Lorimer, D. R., Freire, P., Lyne, A. G., & Manchester, R. N. 2000, ApJ, 535, 975
Chakrabarty, D., & Morgan, E. H. 1998, Natur, 394, 346
Cocozza, G., Ferraro, F. R., Possenti, A., et al. 2008, ApJL, 679, L105
Cohen, M., Wheaton, W. A., & Megeath, S. T. 2003, AJ, 126, 1090
Cordes, J. M., & Lazio, T. J. W. 2002, arXiv:astro-ph/0207156
D'Amico, N., Possenti, A., Manchester, R. N., et al. 2001, ApJL, 561, L89
Deller, A. T., Archibald, A. M., Brisken, W. F., et al. 2012, ApJL, 756, L25
Demorest, P. B., Pennucci, T., Ransom, S. M., Roberts, M. S. E., & Hessels, J. W. T. 2010, Natur, 467, 1081
Edmonds, P. D., Gilliland, R. L., Camilo, F., Heinke, C. O., & Grindlay, J. E. 2002, ApJ, 579, 741
Epchtein, N., Deul, E., Derriere, S., et al. 1999, A&A, 349, 236
Faulkner, A. J., Stairs, I. H., Kramer, M., et al. 2004, MNRAS, 355, 147
Ferraro, F. R., Possenti, A., D'Amico, N., & Sabbi, E. 2001, ApJL, 561, L93
Freire, P. C., Kramer, M., & Lyne, A. G. 2001, MNRAS, 322, 885
Freire, P. C. C., Bassa, C. G., Wex, N., et al. 2011, MNRAS, 412, 2763
Hessels, J. W. T., Roberts, M. S. E., McLaughlin, M. A., et al. 2011, in AIP Conf. Ser. 1357, Radio Pulsars: An Astrophysical Key to Unlock the Secrets of the Universe, ed. M. Burgay et al. (Melville, NY: AIP), 40
Kaplan, D. L., Bhalerao, V. B., van Kerkwijk, M. H., et al. 2013, ApJ, 765, 158
Kaplan, D. L., Stovall, K., Ransom, S. M., et al. 2012, ApJ, 753, 174
Krivonos, R., Tsygankov, S., Revnivtsev, M., et al. 2010, A&A, 523, A61
Kurucz, R. 1993, ATLAS9 Stellar Atmosphere Programs and 2 km/s Grid. Kurucz CD-ROM No. 13 (Cambridge, MA: Smithsonian Astrophysical Observatory), 13
Lazaridis, K., Verbiest, J. P. W., Tauris, T. M., et al. 2011, MNRAS, 414, 3134
Löhmer, O., Kramer, M., Mitra, D., Lorimer, D. R., & Lyne, A. G. 2001, ApJL, 562, L157
Manchester, R. N., Hobbs, G. B., Teoh, A., & Hobbs, M. 2005, AJ, 129, 1993
Minniti, D., Lucas, P. W., Emerson, J. P., et al. 2010, NewA, 15, 433
Monet, D., et al. 1998, VizieR Online Data Catalog, 1252, 0
Monet, D. G., Levine, S. E., Canzian, B., et al. 2003, AJ, 125, 984
Munari, U., Sordo, R., Castelli, F., & Zwitter, T. 2005, A&A, 442, 1127

Nice, D. J., & Taylor, J. H. 1995, ApJ, 441, 429
Nolan, P. L., Abdo, A. A., Ackermann, M., et al. 2012, ApJS, 199, 31
Pallanca, C., Dalessandro, E., Ferraro, F. R., et al. 2010, ApJ, 725, 1165
Papitto, A., Ferrigno, C., Bozzo, E., et al. 2013, Natur, in press (arXiv:1305.3884)
Possenti, A., D'Amico, N., Manchester, R. N., et al. 2003, ApJ, 599, 475
Ransom, S. M. 2001, PhD thesis, Harvard Univ.
Ransom, S. M., Eikenberry, S. S., & Middleditch, J. 2002, AJ, 124, 1788
Ray, P. S., Abdo, A. A., Parent, D., et al. 2012, Proc. 2011 Fermi Symp., in press (arXiv:1205.3089)
Roberts, M. S. E. 2013, in IAU Symp. 291, Neutron Stars and Pulsars, ed. J. van Leeuwen (Cambridge: Cambridge Univ. Press), 127
Romani, R. W., Filippenko, A. V., Silverman, J. M., et al. 2012, ApJL, 760, L36
Romani, R. W., Kerr, M., Craig, H. A., et al. 2011, ApJ, 738, 114
Roming, P. W. A., Kennedy, T. E., Mason, K. O., et al. 2005, SSRv, 120, 95
Saito, R. K., Hempel, M., Minniti, D., et al. 2012, A&A, 537, A107
Shklovskii, I. S. 1970, SvA, 13, 562
Skrutskie, M. F., Cutri, R. M., Stiening, R., et al. 2006, AJ, 131, 1163
Stetson, P. B. 2000, PASP, 112, 925
Tam, P. H. T., Hui, C. Y., Huang, R. H. H., et al. 2010, ApJL, 724, L207
van Kerkwijk, M. H., Breton, R. P., & Kulkarni, S. R. 2011, ApJ, 728, 95
Voges, W., Aschenbach, B., Boller, T., et al. 1999, A&A, 349, 389
Wang, Z., Archibald, A. M., Thorstensen, J. R., et al. 2009, ApJ, 703, 2017
Wijnands, R., & van der Klis, M. 1998, Natur, 394, 344